Backscatter Coefficient Estimation Using Array Transducers

Michael F. Insana, *Member, IEEE,* Timothy J. Hall, *Member, IEEE,* and Larry T. Cook, *Member, IEEE*

Abstract— This paper describes an extension of our broadband method for estimating backscatter coefficients from random media to include data from array transducers. Four different transducer designs have now been considered: one- and two-dimensional linear arrays, annular arrays, and single-element focused pistons commonly used in mechanical sector scanners. The analysis shows that if the backscatter echo spectrum is properly normalized, the shape of the piezoelectric elements affects only the magnitude and not the frequency dependence of the backscatter coefficient estimates. Experimental data were acquired using laboratory and clinical imaging instrumentation to verify the analysis. We compared backscatter coefficients measured as a function of frequency from well-defined scattering media that were obtained using a 1-D linear array and focused piston transducers. Instrument-independent results were found that matched theoretical predictions within the measurement error between 2 and 12 MHz. We conclude from this study that accurate backscatter coefficient estimates may be easily obtained using current clinical imaging instrumentation.

I. INTRODUCTION

TWO PRINCIPAL goals of quantitative analysis in diagnostic ultrasound are to understand the nature of sound-tissue interactions and to identify and develop new diagnostic tools not available with current gray-scale imaging and Doppler techniques. Towards these goals, various approaches to echo signal processing have been proposed to accurately measure acoustic scattering properties of soft tissues [6], [11], [17], [21]–[23], [27], [29], [30]. Although based on the same physical principles, the various methods have produced large variations in reported backscatter coefficient estimates for ostensibly the same tissues, e.g., [26]. In all probability, the tissues were not the same, and the variability in backscatter was due in large part to a variability in the physical state of the tissues examined. Considering that backscatter coefficient estimates vary with the size, number, shape, and elastic properties of the tissue microanatomy, and that these properties can change with the amount of tissue perfusion [13] for *in vivo* measurements and the tissue temperature and post-excision time [2] for *in vitro* measurements, the most meaningful backscatter measurements are those made in live tissues, *in situ.*

The ideal instruments for this task are clinical imaging systems. System features that define high-quality diagnostic
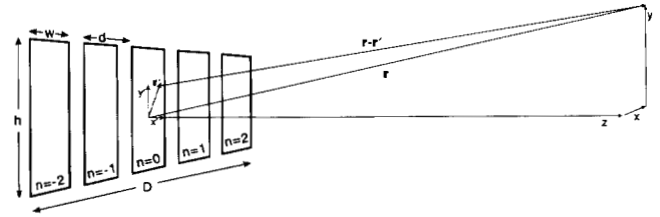
Fig. 1. Transducer geometry for describing field patterns from a 1-D linear array.

imaging also enhance quantitative analysis. The purpose of this paper is to update, clarify, and expand our previous analysis [11] to include data reduction techniques for measuring backscatter coefficients with array transducers. We focus on the use of 1-D linear arrays, annular arrays, and mechanical probe designs to emphasize the possibilities of clinical applications using current technology, although we include a discussion of 2-D linear arrays to show how the imaging technology of the future is also important for quantitative analysis.

The paper begins with a brief review of the principles of acoustic radiation and Fourier optics in order to present a common framework for modeling incident acoustic pressure field patterns for the four transducer designs. Each field pattern is then introduced into the echo spectrum equation to express the backscatter coefficient equation for each transducer design. The results are summarized in two tables and verified experimentally for 1-D linear arrays and focused piston transducers.

II. METHODS

A. Field Patterns

Applying the Huygens-Fresnel principle ([10], section 4.1), we consider the radiating surface of the transducer as a collection of point sources that oscillate sinusoidally. The net pressure field $p_\omega(\mathbf{r}, t)$ at the vector position (bold typeface) $\mathbf{r}$, time t, and temporal frequency $\omega = 2\pi f$, may be determined by summing the pressure fields from the oscillating sources at position $\mathbf{r}'$ (Fig. 1). If the sources lie entirely within the x', y' plane, the radiating surface is defined by the aperture distribution function $a(x', y')$.

The standard Fresnel approximations are applied to restrict the geometry of the experiment and thereby greatly simplify the following analysis ([10], section 4.1). First, the distance between the radiator and observation planes z is much greater than the maximum linear dimension of the radiating area, i.e., $z \gg \text{Max}\{x', y'\}$. Second, only a small region about the beam axis is of concern in the analysis, i.e., the paraxial

approximation, where $z \gg \text{Max}\{x, y\}$. As a result, the pressure field is expressed as

$$p_\omega(\mathbf{r}, t) = P_\omega(t) \frac{\exp(ikr)}{i\lambda z} \mathcal{F}\left\{ a(x', y') \exp\left[\frac{ik}{2z}(x'^2 + y'^2)\right]\right\}$$

(1)

where P_ω is the pressure amplitude, λ is the complex wavelength, $k = \omega/c + i\alpha(\omega)$ is the wavenumber, c is the longitudinal speed of sound, and α is the attenuation coefficient. Also, $\mathcal{F}\{f(x', y')\}$ indicates the 2-D Fourier transform of the function $f(x', y')$:

$$\mathcal{F}\{f(x', y')\} = \iint_{-\infty}^{\infty} f(x', y') \exp\left[-i2\pi(u_x x' + u_y y')\right] dx' dy'$$

for the spatial frequencies $u_x = x/\lambda z$ and $u_y = y/\lambda z$. With these assumptions, the accuracy of (1) is within 3% at a distance 42 mm from a transducer with a 19 mm aperture (see Section II-*I*).

Under the Fresnel approximations, the pressure is proportional to the product of the Fourier transform of the aperture function and a quadratic phase factor. This phase factor must be eliminated to achieve (Fraunhofer) diffraction-limited spatial resolution—and closed-form solutions to equations in the subsequent backscatter analysis—at the range of depths important for diagnostic evaluation of tissues.

B. 1-D Linear Arrays

In the near field of the beam, the quadratic phase factor may be eliminated by focusing. For example, a cylindrical acoustic lens placed on the radiating surface ($z = 0$) of a 1-D array will focus the beam in elevation (along the y axis in Fig. 1), and an electronic 'lens' may be used to focus in azimuth (along the x axis).

Weakly focusing in elevation, e.g., using a plano-convex acoustic lens, introduces the phase factor $\exp[ik(\Delta_y - y'^2/2R)]$, where R is the focal length of the lens, $\Delta_y = R_y - \sqrt{R_y^2 - h^2/4}$ is its thickness, R_y is the radius of curvature of the lens, and h is the height of the radiating element ([10], section 5.1).

The beam is weakly focused in azimuth electronically by delaying the transmission and reception of the signals. Electronic focusing introduces the phase factor $\exp[ik(\Delta_x - \psi x'^2] = \exp(i\omega\tau_n)$, where the time delay, τ_n, across the $-N/2 \leq n \leq N/2$ array elements is of the form [18]

$$\tau_n = T - \psi(nd)^2/c \ .$$

(2)

$T = \Delta_x/c$ is a constant time delay applied to each element, $nd = x'$ is the position of the nth element in the plane of the radiator (Fig. 1), and ψ is a focusing factor. The transducer is focused in azimuth for a depth z by adjusting the constants T and ψ. If ψ is adjusted during signal transmission and reception such that $\psi = 1/2R$, then

$$p_\omega(\mathbf{r}, t) = P_\omega(t) \frac{\exp[ik(r + \Delta_x + \Delta_y)]}{i\lambda R} \mathcal{F}\{a(x', y')\}$$

(3)

and we obtain Fraunhofer diffraction-limited resolution at $z = R$. The aperture distribution function a and its Fourier transform $\mathcal{F}\{a\}$ for a 1-D array whose elements radiate with equal amplitude are given in Table I.

Like single-element transducers, the elevational focal length of 1-D linear arrays is fixed. Therefore, it is necessary to limit the range of echo signals used to estimate backscatter coefficients to a region about the elevational focal length if we are to obtain simple, closed-form solutions. Alternatively, 2-D linear arrays, and to a lesser degree annular arrays, provide adjustable electronic focusing for a broad range of depths z in the medium.

C. 2-D Linear Arrays

Improved spatial resolution and adjustable focal lengths are possible with 2-D array transducers. Assume an $N \times N$ array of square ($w \times w$) radiating elements are separated by the center-to-center distance d in both azimuth, $x' = nd$, and elevation, $y' = md$, where n and m are integers. The radiating surface area is $A = (Nw)^2 = (Dw/d)^2$, and the array dimensions are $D \times D$.

The time delay at each element (n, m) required to focus the beam at range z is given by [18]

$$\tau_{nm} = T - \left[\psi(nd)^2 + \xi(md)^2\right]/c.$$

(4)

The first term, T, is a constant delay applied to all elements. The second and third terms are variable time delays across elements in azimuth and elevation, respectively.

The principal advantage of a 2-D array is the flexibility to focus in three dimensions at (virtually) any range. Variable delays are applied to eliminate the quadratic phase factor in (1) at specific depths in the medium by adjusting the delay factors ψ and ξ, so that $\psi = 1/2z = \xi$, and we obtain the Fraunhofer diffraction-limited resolution of (3). The aperture function for the 2-D linear array and its Fourier transform are listed in Table I. Of course, there are obvious and severe difficulties implementing 2-D arrays that are related to the extraordinary number of transmit and receive channels needed for a practical system [28].

D. Annular Arrays

Annular array transducers combine the superior 3-D spatial resolution of single-element focused piston radiators with the variable focal length of 1-D linear arrays. An aperture containing N annuli, each of width w and center-to-center distance d, will have a total diameter $D = 2w[1 + (N-1)d/w]$, a nominal area $A' = \pi D^2/4$, and a total radiating-surface area $A = \pi w^2 N[1 + (N-1)d/w]$.

To focus the beam, signal transmission and reception is delayed according to (2), but for an annular array $nd = r' = \sqrt{x'^2 + y'^2}$. If we again adjust ψ so that $\psi = 1/2z$ for each depth that we obtain data, the pressure field is also given by (3), where Δ_r is used in place of $\Delta_x + \Delta_y$. The focal properties should be statically adjustable for backscatter measurements, i.e., the dynamic focusing used for imaging is not required.

Near the focal length, (3) describes the incident pressure field for each of the transducers. It is the aperture distribution

TABLE I
APERTURE DISTRIBUTION FUNCTIONS AND THEIR FOURIER TRANSFORMS ARE LISTED FOR FOUR TRANSDUCER DESIGNS. RESULTS FOR UNIFORMLY WEIGHTED AND GAUSSIAN-APODIZED FOCUSED PISTON APERTURES ARE INCLUDED. UNIFORMLY WEIGHTED APERTURES ARE ASSUMED EXCEPT WHERE INDICATED.

Transducer	Aperture Distribution Function, $a(x', y')$		Aperture Area
1D Linear Array	$\frac{1}{A}\left\{\left[\text{rect}\left(\frac{x'}{D}\right)\frac{1}{d}\text{comb}\left(\frac{x'}{d}\right)\right]\otimes\left[\text{rect}\left(\frac{x'}{w}\right)\right]\right\}\text{rect}\left(\frac{y'}{h}\right)$		$A = Dwh/d$
2D Linear Array	$\frac{1}{A}\left\{\left[\text{rect}\left(\frac{x'}{D}\right)\frac{1}{d}\text{comb}\left(\frac{x'}{d}\right)\right]\otimes\left[\text{rect}\left(\frac{x'}{w}\right)\right]\right\}$ $\times\left\{\left[\text{rect}\left(\frac{y'}{D}\right)\frac{1}{d}\text{comb}\left(\frac{y'}{d}\right)\right]\otimes\left[\text{rect}\left(\frac{y'}{w}\right)\right]\right\}$		$A = (Dw/d)^2$
Single Element Focused Piston	$\frac{1}{A}\text{circ}\left(\frac{r'}{D}\right)$	$\frac{2}{A}\exp(-2\pi r'^2/A)$ (apodized)	$A = \pi D^2/4$
Annular Array	$\frac{1}{\pi w^2}\text{circ}\left(\frac{r'}{2w}\right)$ $+\sum_{n=2}^{N}\frac{1}{A_n}\left\{\text{circ}\left(\frac{r'}{2r_{2,n}}\right)-\text{circ}\left(\frac{r'}{2r_{1,n}}\right)\right\}$		$A_n = \pi w^2\left[1 + 2(n-1)\frac{d}{w}\right]$ $N = $ Number of elements

Transducer	$\mathcal{F}\{a(x', y')\}$		Definitions
1D Linear Array	$\left[\sum_{n=-\infty}^{\infty}\text{sinc}\,(wu_x)\,\text{sinc}\left(Du_x - \frac{nD}{d}\right)\right]\text{sinc}\,(hu_y)$		$u_y = y/\lambda z$ $u_x = x/\lambda z$
2D Linear Array	$\left[\sum_{n=-\infty}^{\infty}\text{sinc}\,(wu_x)\,\text{sinc}\left(Du_x - \frac{nD}{d}\right)\right]$ $\times\left[\sum_{n=-\infty}^{\infty}\text{sinc}\,(wu_y)\,\text{sinc}\left(Du_y - \frac{nD}{d}\right)\right]$		$\text{circ}\left(\frac{r}{R}\right) = \begin{cases} 1 & r \le R/2 \\ 0 & \text{otherwise} \end{cases}$
Single Element Focused Piston	$2J_1\,(\pi Du_r)\,/\pi Du_r$	$\exp\left[(\pi Du_r)^2/8\right]$ (apodized)	$u_r = r/\lambda z$ $r^2 = x^2 + y^2$
Annular Array	$\frac{J_1(2\pi wu_r)}{\pi wu_r}$ $+\sum_{n=2}^{N}\left\{\frac{J_1(2\pi r_{2,n}u_r)}{\pi r_{2,n}u_r} - \frac{J_1(2\pi r_{1,n}u_r)}{\pi r_{1,n}u_r}\right\}$		$r_{1,n} = (n-1)d$ $r_{2,n} = [w + (n-1)d]$

function $a(x', y')$ that distinguishes the backscatter analyses for the various transducers described above. These functions and their corresponding Fourier transforms are summarized in Table I for four transducer designs. We have included results for a uniformly weighted single-element focused piston transducer as discussed in our previous work [11] and for a Gaussian-apodized single-element focused piston as discussed by others [6], [30], [29]. Note that if the elements in an annular array are contiguous, the aperture distribution function for annular arrays and its Fourier transform are identical with those for single-element focused pistons of equal f-number.

E. Echo Signal Spectrum

We have shown previously that the Fourier transform of the echo signal from a random medium that scatters sound, $S_m(k)$, near the focal length of the transducer, R, may be expressed as a function of the wave number k, by the following expression ([11], (31)):

$$S_m(k) = \frac{A^2 k^3 C(k)\exp(i2kR)}{i(2\pi R)^2}\iiint_{-\infty}^{\infty} H^2(x_0, y_0)$$
$$\times g(z_0)\gamma(\mathbf{r_0})\exp(i2kr_0)\,dx_0dy_0dz_0 \tag{5}$$

The factor $C(k) = -\frac{1}{2}\rho cT_\omega U_\omega$ is the frequency response of the instrumentation, which includes the acoustoelectric transfer function T_ω, while $g(z_0)$ and $\gamma(\mathbf{r_0})$ are the range gate and scattering source functions for the medium, respectively. The function $\gamma(\mathbf{r_0})$ describes the fluctuation in the density and compressibility of the propagating medium that scatter the sound, which are the properties we seek to characterize by this analysis. We define $H(x_0, y_0) \equiv \mathcal{F}\{a(x', y')\}$ as the transducer beam directivity function at the focal length $z = R$ (Table I). Although the integration is over an infinite volume, the actual volume that produces backscatter at any instant of time — the scattering volume V — is determined by the pulse length, range gate, and directivity function. We have also set $r + \Delta_x + \Delta_y = R$. Finally, because of the paraxial approximation, we find it convenient to shift the coordinate system to the center of the scattering volume, where we define $r_0 = \sqrt{x^2 + y^2 + (z - R)^2}$ with the aid of Fig. 2.

F. Reference Signal Spectrum

A reference signal is included in the analysis to remove the frequency-dependent instrument effects from those of the scattering medium. We chose the echo from pulses traveling in water that are normally incident on a planar surface as our
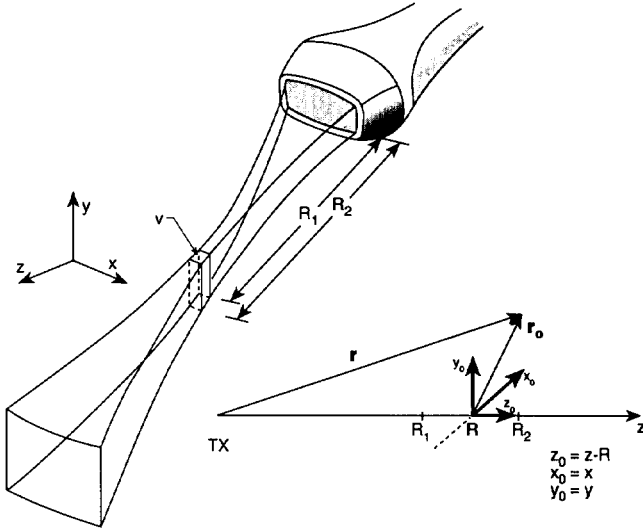
Fig. 2. Coordinate system used for derivation of the echo spectrum.

reference. The scattering function for a reflecting plane with amplitude reflection coefficient γ' is

$$\gamma(\mathbf{r_0}) = \gamma' \, h_\gamma(z_0), \tag{6}$$

where $h_\gamma(z_0)$ is a step function [4]. In the water $\gamma(\mathbf{r_0}) = 0$, but in the material of the reflector $\gamma(\mathbf{r_0}) = \gamma'$. The discontinuity is in the x, y plane at the center of the range gate located at $z = R$, the focal length of the transducer. Substituting (6) into (5) and assuming local plane waves at R —a consequence of the paraxial approximation—the reference signal spectrum, $S_0(k)$, is given by

$$S_0(k) = \frac{A^2 k^2 C(k) \exp(i2kR)}{(2\pi R)^2}$$
$$\times \frac{k\gamma'}{i} \int_{-\infty}^{\infty} g(z_0) \, h_\gamma(z_0) \exp(i2kz_0) \, dz_0$$
$$\times \iint_{-\infty}^{\infty} H^2(x_0, y_0) \, dx_0 dy_0.$$

First, we compute the 1-D Fourier transform in the range direction. Provided that the range gate, $g(z_0)$, is centered at R and is of length $L = R_2 - R_1$ (Fig. 2) sufficient to encompass the entire reflected pulse, the value of L is immaterial. Assuming a rectangular gate with unit magnitude and infinite length, we find by the derivative theorem [4] that

$$\frac{k\gamma'}{i} \int_{-\infty}^{\infty} g(z_0) \, h_\gamma(z_0) \exp(i2kz_0) dz_0$$
$$= \left(\frac{k\gamma'}{i}\right)\left(\frac{i}{2k}\right) \int_{-\infty}^{\infty} \frac{dh_\gamma(z_0)}{dz_0} \exp(i2kz_0) dz_0$$
$$= \frac{\gamma'}{2} \int_{-\infty}^{\infty} \delta(z_0) \exp(i2kz_0) \, dz_0 = \frac{\gamma'}{2}. \tag{7}$$

Second, the 2-D integral of the directivity function is found by applying Parseval's theorem ([10], p. 10):

$$\iint_{-\infty}^{\infty} H^2(x_0, y_0) \, dx_0 dy_0$$

$$= (\lambda R)^2 \iint_{-\infty}^{\infty} |H(u_x, u_y)|^2 \, du_x du_y$$
$$= (\lambda R)^2 \iint_{-\infty}^{\infty} |a(x', y')|^2 \, dx' dy'$$
$$= \frac{(\lambda R)^2}{A} = \frac{(2\pi R)^2}{k^2 A}, \tag{8}$$

where the spatial frequency variables $u_x \equiv x/\lambda z = x_0/\lambda R$ and $u_y \equiv y/\lambda z = y_0/\lambda R$. (Note that H is real, Table I.) The reference spectrum therefore reduces to

$$S_0(k) = \frac{A\gamma' C(k)}{2} \exp(i2kR) \ , \tag{9}$$

and is the same for each of the transducer designs listed in Table I.

G. Normalized Power Density Spectrum

The average power density within the time interval T_L (corresponding to the range gate $L = \frac{1}{2}cT_L$) is $\langle |S_m(k, L)|^2 \rangle / L$ for the test medium and $\langle |S_0(k, L)|^2 \rangle / L$ for the reference medium [3]. The angle brackets $\langle \cdot \rangle$ indicate the operation of taking the ensemble average of the random variable within. In practice, we obtain N_ℓ statistically independent spectra from a region in an isotropic, random medium and compute

$$\frac{1}{L}\langle |S(k, L)|^2 \rangle = \frac{1}{LN_\ell} \sum_{\ell=1}^{N_\ell} |S_\ell(k, L)|^2 \ .$$

The normalized power density spectrum $W(k)$ is defined as

$$W(k) = \left(\frac{\gamma'}{2}\right)^2 \frac{\langle |S_m(k, L)|^2 \rangle}{\langle |S_0(k, L)|^2 \rangle} \exp\left(4[\alpha_m(\omega) - \alpha_0(\omega)]R\right) \tag{10}$$

where $\alpha_m(\omega)$, and $\alpha_0(\omega)$ are the attenuation coefficients for the test medium and reference medium (water). Combining (5), (9), and (10), we find that

$$W(k) = \frac{A^2 k^6}{(2\pi R)^4} \iiint_{-\infty}^{\infty} \iiint_{-\infty}^{\infty}$$
$$\times H^2(x_0, y_0) H^2(x_1, y_1) g(z_0) g(z_1)$$
$$\times \langle \gamma(\mathbf{r_0}) \gamma(\mathbf{r_1}) \rangle \exp(i2k(r_0 - r_1))$$
$$\times dx_0 dy_0 dz_0 dx_1 dy_1 dz_1, \tag{11}$$

where $\mathbf{r_0}$ and $\mathbf{r_1}$ are two positions in the scattering volume.

Assuming that the echo signal can be described as a weakly stationary random process [3], the power density spectrum becomes a function of one position variable, the difference vector $\Delta\mathbf{r} = \mathbf{r_0} - \mathbf{r_1}$, and (11) reduces to

$$W(k) = \frac{A^2 k^6}{(2\pi R)^4} \iiint_{-\infty}^{\infty}$$
$$\times B_H(\Delta x, \Delta y) B_g(\Delta z) B_\gamma(\Delta r)$$
$$\times \exp(i2k\Delta r) d\Delta x d\Delta y d\Delta z \tag{12}$$

where $\Delta r = \sqrt{(\Delta x)^2 + (\Delta y)^2 + (\Delta z)^2}$, and $B_H(\Delta x, \Delta y)$, $B_g(\Delta z)$, and $B_\gamma(\Delta r)$ are autocorrelation functions for the directivity, range gate, and (isotropic random) scattering medium functions, respectively, [6], [11], [15], [17].

TABLE II
BACKSCATTER COEFFICIENT FUNCTIONS ARE LISTED FOR FOUR TRANSDUCER DESIGNS. THESE FUNCTIONS RESULT FROM THE COMBINATION OF (15) WITH VALUES FOR THE AUTOCORRELATION OF THE DIRECTIVITY FUNCTION AT ZERO LAG, $B_H(0,0)$, THE AREA OF THE RADIATING TRANSDUCER SURFACE, A, AND THE NOMINAL AREA OF THE APERTURE, A'. UNIFORMLY WEIGHTED APERTURES ARE ASSUMED EXCEPT WHERE OTHERWISE INDICATED.

Transducer	σ_b		$B_H(0,0)$		Aperture Area
1D Linear Array	$\frac{3d^2R^2}{2w^2LA'}W(k)$		$(\frac{2}{3}\lambda R)^2/A'$		$A = Dwh/d$ $A' = Dh$
2D Linear Array	$\frac{3d^4R^2}{2w^4LA'}W(k)$		$(\frac{2}{3}\lambda R)^2/A'$		$A = (Dw/d)^2$ $A' = D^2$
Single Element Focused Piston	$\frac{4R^2}{(0.919)3LA'}W(k)$	$\frac{4R^2}{3LA'}W(k)$ (apodized)	$0.919(\lambda R)^2/2A$	$(\lambda R)^2/2A$ (apodized)	$A = \pi D^2/4 = A'$
Annular Array	$\frac{4R^2A'}{(0.919)3LA'^2}W(k)$		$0.919(\lambda R)^2/2A$		$A = \pi w^2 N\left[1+(N-1)\frac{d}{w}\right]$ $A' = \pi D^2/4$

H. Backscatter Coefficient

Equation (12) shows that the backscatter power density spectrum is proportional to the 3-D Fourier transform of a product of autocorrelation functions. To simplify, we assume that B_γ becomes negligibly small as Δr is increased before either B_H or B_g changes significantly [15], [17], [29], [30]. Then B_H and B_g are nearly constant and equal to their value at $\Delta r = 0$. (It is primarily the beam width that restricts the size of scatterers for which the approximation holds. At 5 MHz and $f/2$, for example, the beam width is $\sim 600\mu m$.) Consequently,

$$W(k) \simeq \frac{A^2 k^6}{(2\pi R)^4}B_H(0,0)B_g(0)\iiint_{-\infty}^{\infty}$$
$$\times B_\gamma(\Delta r)\exp(i2k\Delta r)d\Delta x d\Delta y d\Delta z$$
$$= \left(\frac{Ak}{\pi R^2}\right)^2 B_H(0,0)B_g(0)\sigma_b(k) \tag{13}$$

where

$$\sigma_b(k) = \frac{k^4}{16\pi^2}\iiint_{-\infty}^{\infty}B_\gamma(\Delta r)\exp(i2k\Delta r)d\Delta x d\Delta y d\Delta z \tag{14}$$

defines the backscatter coefficient in terms of properties of the random medium [14].

It is straightforward to show that $B_g(0)$ is equal to L if a rectangular window is applied to the echo waveform and $3L/8$ if a Hanning window is applied [3]. We have used a Hanning window throughout this paper, although the choice of window function does not significantly affect backscatter coefficient estimates. Spectral distortion is most significant near the bandwidth limits for short waveform segments [1].

From (13), we find an expression for the backscatter coefficient in terms of experimental parameters:

$$\sigma_b(f) = \frac{2}{3L}\left(\frac{\lambda R^2}{A}\right)^2\frac{W(f)}{B_H(0,0)} \tag{15}$$

where the temporal frequency variable f was substituted for the spatial frequency variable k using the relation $k = 2\pi f/c$. The shape of the radiator is reflected in the factors A and B_H.

Separate values for $B_H(0,0)$ are needed to compute the backscatter coefficient for each transducer design. Near the focal plane of a 1-D linear array, for example, we find using Table I that

$$B_H(0,0) = \iint_{-\infty}^{\infty}H^4(x'',y'')dx''dy''$$
$$= \iint_{-\infty}^{\infty}\left[\text{sinc}\left(\frac{wx''}{\lambda R}\right)\sum_{n=-\infty}^{\infty}\right.$$
$$\left.\times\text{sinc}\left(\frac{Dx''}{\lambda R}-\frac{nD}{d}\right)\right]^4\text{sinc}^4\left(\frac{hy''}{\lambda R}\right)dx''dy'' \tag{16}$$
$$\simeq\left[\int_{-\infty}^{\infty}\text{sinc}^4\left(\frac{Dx''}{\lambda R}\right)dx''\right]$$
$$\times\left[\int_{-\infty}^{\infty}\text{sinc}^4\left(\frac{hy''}{\lambda R}\right)dy''\right] \tag{17}$$
$$= \frac{(\frac{2}{3}\lambda R)^2}{A'}. \tag{18}$$

where $A' = Dh$. Equation (17) is an approximation of (16) for contiguous array elements, i.e., $w/d = 1$, that provides the closed-form solution of (18). The assumption is necessary since often we don't know the exact element separation on transducers used clinically, and reasonable because the difference between (16) and (18) is small enough to ignore under practical conditions [32]. As shown in Fig. 3, the error in $B_H(0,0)$ that is introduced by the use of (18) is less than 5% for $w/d \geq 0.7$.

Expressions for σ_b, B_H, and aperture areas are listed in Table II for four transducer designs.

I. Experimental Methods

We verified the accuracy of the above backscatter analysis by comparing values of σ_b predicted by scattering theory with measurements obtained from well-defined scattering media. Two of the four transducer designs summarized in Tables I and II—the 1-D linear array and the focused piston—were studied experimentally.

Two different test media were examined. Both contained a narrow diameter distribution of glass microspheres (Duke Scientific Corp., Palo Alto CA) in an agar suspension (#A360 from Fisher Scientific, Fair Lawn, NJ). The average sphere
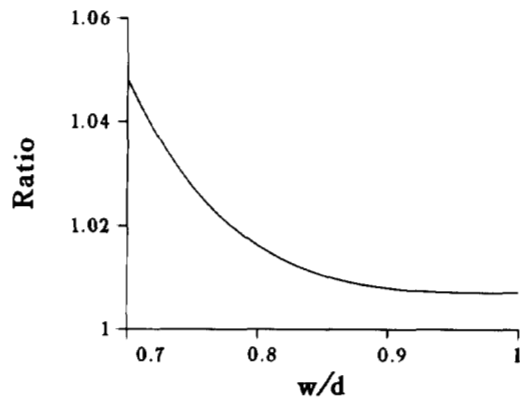
Fig. 3. Ratio of exact (16) and approximate (18) expressions for $B_H(0,0)$ as a function of the gap between array elements as described by w/d. The result shows that even if the gap is as large as $0.3w$, the error in B_H, and therefore σ_b, is less than 5%.

Fig. 4. Diagram of the assembled clinical measurement system as set up to measure reference signals from a fluid interface.

diameter in sample 1 was 41 μm, the standard deviation of the distribution was 2 μm, and the number density was 24.2 spheres per mm^3. The values for sample 2 are 85 μm, 3 μm, and 12.1 spheres per mm^3. Test samples were prepared as described by Madsen *et al.* [20], and wrapped in 13.7 μm-thick plastic sheets (Saran Wrap, DowBrands Inc., Indianapolis, IN) for measurement in water. We compensated for transmission losses through the thin plastic layers by dividing backscatter power spectra by the frequency-dependent transmission coefficient, assuming the sound waves were normally incident (see (6.13) in [16], where for the plastic $\rho = 1.7$ g/cm^3 and $c = 2504$ m/s).

The speed of sound (c) and attenuation coefficients ($\alpha(f) = \alpha' f^\eta$) were measured at 21°C for sample 1 ($c = 1542$ m/s, $\alpha' = 0.2$ dB cm^{-1} MHz$^{-1.3}$, $\eta = 1.3$) and sample 2 ($c = 1550$ m/s, $\alpha' = 0.2$ dB cm^{-1} MHz$^{-1.3}$, $\eta = 1.3$) using a narrow-band substitution technique [19].

Laboratory and clinical imaging systems were both used to record echo waveforms from the test media. The *clinical imaging system* included a Quantum 2000 (Siemens Ultrasound, Inc., Issaquah, WA) and a 5L45 *linear array transducer* (without wedge). The assembled clinical system is illustrated in Fig. 4. This commercial imaging system has been modified by the manufacturer to provide access to analog radio-frequency (RF) echo signals and the frame, beam, and pulse synchronization signals. These signals are received by a digital gate device built in our laboratory [33] that is used to access echo waveforms prior to any nonlinear signal processing. The digital gate enabled us to record signals from any user-selected region of interest. That region is displayed in the image as a white box by feeding the appropriate signals back into a video port. Echo waveforms were low-pass filtered, digitized at a rate of 50 Msamples per second, and stored on hard disk for later processing.

This particular 5L45 linear array had a 4.5 MHz center frequency, a 4.5 MHz bandwidth (-20 dB), and used a Gaussian apodization function on transmit. The data were analyzed assuming no apodization of the array on transmission or reception. (In this context, *apodization* refers to unequal weighting of the contribution from elements within the active aperture during beam formation.) We selected a transmit focus
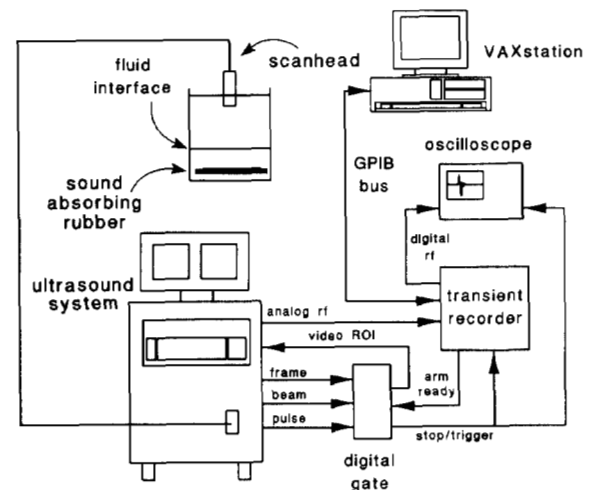
in azimuth to equal the geometric focus in elevation (~ 4.2 cm). The output power was set to maximum (system display setting was -7 dB), the time-gain compensation amplifier was set to minimum at all depths, and the overall gain was set to -17 dB for sample 1 and -27 dB for sample 2. Gain settings were adjusted to fully use the dynamic range of the digitizer. Sample and reference waveforms were recorded at the same gain settings for each sample. Test samples were scanned in distilled and degassed water at 21°C. The center of each sample was positioned at the focal length. Twenty-five consecutive waveform segments, each 10 μs in duration, were recorded per frame cycle. Ten such data sets were recorded per sample after translating the transducer in a direction perpendicular to the beam axis a distance of 5 mm between recordings.

A *laboratory system* described previously [11] was used to record echo signals from a uniformly-weighted *single-element focused piston transducer*. This system included a 10 MHz circular transducer (Panametrics V315, 9.6 MHz center frequency, 13 MHz bandwidth (-20dB), Waltham MA) with a 19 mm diameter that was spherically focused at 55.2 mm. The reference signals for the laboratory system were pulses reflected from a polished Lucite block placed in water (21°C) normal to the beam axis at the focal length.

There is an important distinction between the laboratory and clinical systems. In the laboratory, a calibrated attenuator reduced the output of the transducer (but not the echo signal) to match the amplitude of the reference signals to that from the test media. Signal matching enabled us to use the entire 8-bit dynamic range of the transient recorder for all signals recorded. Unfortunately, this clinical instrument did not provide the same access to the pulser circuitry possible in the laboratory, so that reflected signals from the Lucite block were too strong. Changing the receiver gain between recordings of the sample and reference signals is not an option, since that could reintroduce a frequency-dependent instrument effect. Instead we used pulses reflected from a water—carbon tetrachloride interface as a reference signal (Fig. 4). The reflection coefficient of the interface between the immiscible fluids is much smaller than that at a water—Lucite interface, and it may be adjusted
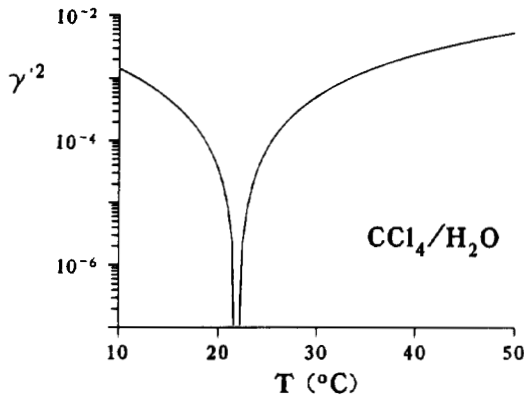
Fig. 5. The intensity reflection coefficient, γ'^2, for a CCl_4 —water interface is plotted as a function of temperature.

by changing the temperature. From temperature-dependent values of density and sound speed [34], we computed γ'^2 [(6.7a) in [16]] and plotted the results in Fig. 5. Precise temperature control is required near room temperature, where the reflections are weakest. At the $23.5 \pm 0.1°C$ temperature of this reference signal measurement, the uncertainty in γ'^2, and therefore the bias in σ_b, was as high as 13.8%. Increasing the temperature of the fluids to $25.0 \pm 0.1°C$ could have reduced this bias by one half.

The simplicity of the test media enabled us to predict backscatter coefficients for comparison with measurements. The method of Faran [8] was used to predict backscatter coefficients from the test media as a function of frequency. Because the accuracy of Faran's theory has been verified for simple scattering media [5], [8], it has been used as a comparison standard for testing the accuracy of backscatter measurement techniques [21]. The essential parameters for applying Faran's theory to predict backscatter coefficients are mass density (1.00 g/cm^3 for the agar and 2.38 g/cm^3 for glass spheres), longitudinal sound speed (5571.9 m/s for glass), and Poisson's ratio (0.21 for glass) [21]. The mean sphere diameters and number densities listed above were used in the computations.

III. RESULTS AND DISCUSSION

Measured and predicted backscatter coefficients are plotted as a function of frequency for samples 1 and 2 in Fig. 6. An overall agreement between experiment and theory is demonstrated. The linear array transducer and clinical instrumentation permit backscatter measurements between 3 MHz and 7 MHz. The higher center frequency and increased bandwidth of the focused piston and laboratory instrumentation extended the measurements up to 12 MHz.

Despite agreement within the uncertainty of the measurement, the linear array data displays a tendency to be somewhat greater than that of the focused piston. We investigated the possibility that this was a consequence of ignoring the effects of apodization in the data reduction. In their analysis of piston radiators, Ueda and Ozawa [29] showed that the normalized backscatter power density spectrum from a Gaussian-apodized piston radiator is 0.36 dB greater than that of a uniformly-
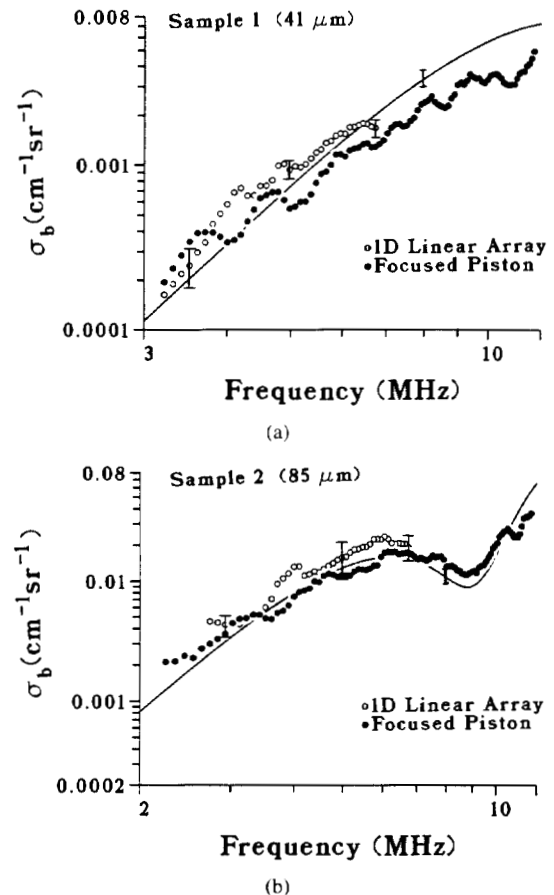

(a)

(b)

Fig. 6. Backscatter coefficients versus frequency, $\sigma_b(f)$, are plotted for two test samples and two transducer geometries. Measurements are compared with theoretical predictions (solid lines) between 2 and 12 MHz. Error bars on points indicate $\pm$ one standard error. Error bars on the curves at 8 MHz are an estimation of the uncertainty in the predictions based on the variability in glass sphere diameters.

weighted aperture — hence the additional factor of 0.919 in the expression for σ_b in Table II. We have not found the appropriate analytic expressions for apodized arrays, although it is reasonable to assume that the results are similar to that for focused pistons, i.e., the normalized echo spectrum is slightly greater for apodized arrays. The wide variety of apodization strategies now used in commercial imaging systems coupled with the small effect on the backscatter coefficient estimation suggest that apodization can be ignored in quantitative analysis with little consequence. The apparent bias in Fig. 6 is most likely caused by the relatively large uncertainty in the reference signal amplitude.

We also measured backscatter as a function of the range gate duration. In Fig. 7, the integrated backscatter coefficient (IBC = $\left[\sum_{f_1}^{f_2} \sigma_b(f)\right]/(f_2 - f_1)$ [12]) from 3.0 to 7.0 MHz is shown to be independent of gate duration. IBC values were used to summarize changes in σ_b from a single value. One set of 25 echo waveforms was used for the focused piston data (solid circles) at all gate durations. Analogous measurements were obtained for the linear array (open circles). However, ten independent sets of echo waveforms were used to compute a second set of IBC values for the linear array (open squares). The three curves in Fig. 7 lead us to conclude that σ_b estimates
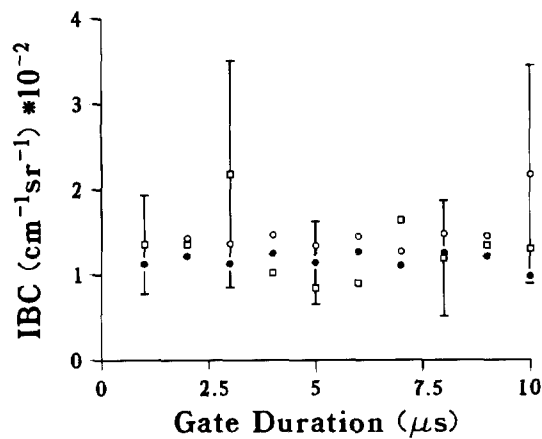
Fig. 7.   Plots of the integrated backscatter coefficient (IBC) versus frequency indicate that the measurements are unbiased for a broad range of gate durations. Error bars indicate ± one standard error.

are independent of the gate length for $1.0\mu s \leq T_L \leq 10.0\mu s$, corresponding to submillimeter axial resolution. Of course, the variance in σ_b estimates is much greater than the variance in echo amplitude estimates, so that, at comparable spatial resolution, backscatter coefficient imaging is much noisier than conventional B-mode imaging [12], [31].

Thus far we have not considered phased array transducers because of such well-known problems as the reduction in effective aperture and growth of grating lobes that are encountered when the beam is electronically steered. Such complicating factors can be incorporated into the above analysis by including the excellent analysis of phased arrays given by Macovski [18]. However, beam steering is not an essential feature of quantitative analysis.

To be an effective diagnostic tool, quantitative backscatter analysis must be fast, flexible, and accurate. With our approach, data are acquired near the focal region of the transducer, and simple closed-form expressions are used to quickly yield accurate σ_b estimates. We depend on the instrumentation to focus the beam at the region of interest, and to thus provide the flexibility required for clinical applications. Alternatively, the data reduction method of Madsen *et al.* [20], [21] provides the flexibility to obtain accurate backscatter coefficient estimates at any range, but is very computationally intensive. The addition of a random reference medium (to replace the plane reflector) has been shown by Zagzebski *et al.* [31] to significantly reduce the processing time of the Madsen technique without compromising accuracy. Others have also successfully used random reference media to normalize backscatter power spectra [25]. Advances in adaptive beamforming methods are now providing large focal regions for backscatter coefficient analysis, which tend to negate differences in the speed, accuracy, and flexibility between the two approaches discussed above. As with imaging, the accuracy of both backscatter coefficient methods decreases in the presence of wave distortions, since accurate models of the beam are integral parts of the analyses.

The future of diagnostic ultrasound technology for imaging and quantitative analysis includes 2-D arrays because of the flexibility they offer. With 2-D arrays, the focal region

may be extended to include the entire field, and correction algorithms may be applied to compensate for wave front distortions [9]. If it becomes possible to implement fully-populated rectangular 2-D arrays, then the backscatter analysis as summarized in Table II is straightforward. However, to reduce electronic complexity, investigators are using sparse geometries with randomly positioned active element locations [7], and obtaining promising results for B-mode imaging. The pressure fields from random sparse arrays may not have closed-form solutions, and therefore the processing speed is decreased when it is necessary to numerically compute fields for each configuration. To determine the utility of quantitative methods for diagnosis, we must continue to search for the right balance among processing speed, flexibility, and measurement accuracy.

IV. CONCLUSION

Analytic expressions for backscatter coefficients were developed for four transducer designs, including linear and annular arrays. The data reduction formulas account for the shape of the radiating elements by introducing frequency-independent factors into the equations, thus providing an accurate and instrument-independent estimation of σ_b. Since *normalized* echo spectra for different transducer designs have the same shape, accurate estimates of parameters that depend on the magnitude of the backscatter coefficient, e.g., IBC, require careful consideration of the transducer geometry. Conversely, parameters determined from the frequency dependence of backscatter and not the absolute magnitude, e.g., scatterer size estimates [12], [17], may be estimated without consideration of the transducer geometry. As with mechanical sector probes, measurements using 1-D arrays are limited to a fixed range of depths in the medium near the focal length. The ability to vary the transmit and receive foci, suggests that annular arrays are the best choice of transducer design for quantitative analysis using current technology. Quantitative backscatter analysis for diagnosis continues to be limited by the unavailability of essential electronic signals in most commercial systems, difficulties in estimating attenuation coefficients in live tissues, and wave front distortions of the pressure fields.

GLOSSARY

$a(x', y')$	aperture distribution function
A	active area of the transducer
A'	nominal area of the transducer
B_H, B_g, B_γ	autocorrelation functions for beam directivity, range gate, and scattering source functions
c	longitudinal speed of sound
C	frequency response of the backscatter instrumentation
$\mathrm{comb}(x)$	$\sum_{n=-\infty}^{\infty} \delta(x - n)$
d	center-to-center distance between array elements (pitch)
D	transducer dimension
f	temporal frequency variable
g	range gate function

h	height of array elements
h_γ	step function
H	transducer beam directivity function
IBC	integrated backscatter coefficient
k	wavenumber
L	range gate length
$\hat{\mathbf{n}}, \hat{\mathbf{r}}$	unit vectors
N	number of array elements
N_ℓ	number of echo signal waveforms
p_ω	acoustic pressure field
P_ω	pressure amplitude
$\mathbf{r}$	vector field position relative to the transducer center, $r = \sqrt{x^2 + y^2 + z^2}$
$\mathbf{r}'$	vector position on transducer surface relative to the center, $r' = \sqrt{x'^2 + y'^2 + z'^2}$
$\mathbf{r_0}, \mathbf{r_1}$	vector field positions relative to the scattering volume center, $r_0 = \sqrt{x^2 + y^2 + (z - R)^2}$
$\Delta\mathbf{r}$	$\mathbf{r_0} - \mathbf{r_1}$
R	focal length
R_y	radius of curvature in elevation (y-axis)
$\mathrm{rect}\left(\frac{x}{X}\right)$	$\begin{cases} 0 & \|x\| > X/2 \\ 1/2 & \|x\| = X/2 \\ 1 & \|x\| < X/2 \end{cases}$
S_0, S_m	Fourier transforms of the echo signals from reference, test media
T	constant time delay
T_L	range gate duration
T_ω	acoustoelectric transfer function
u_x, u_y	spatial frequency variables
w	width of array elements
W	normalized power density spectrum
α_0, α_m	attenuation coefficients in the reference, test media (cm^{-1})
Δ_x, Δ_y	lengths corresponding to the maximum time delays introduced by a lens
γ	scattering source function
γ'	amplitude reflection coefficient
λ	wavelength
ρ	mass density of propagating medium
σ_b	backscatter coefficient
τ_n	time delay applied to the nth array element
ω	(radial) temporal frequency variable
ψ, ξ	time delay factors

ACKNOWLEDGMENT

REFERENCES

[1] M. Akita and M. Ueda, "The effect of windowing on spectral estimation of echoes scattered by a random medium," *J. Acoust. Soc. Amer.*, vol. 83, pp. 1243-1248, 1988.

[2] J. C. Bamber, M. J. Fry, C. R. Hill, and F. Dunn, "Ultrasonic attenuation and backscattering by mammalian organs as a function of time after excision," *Ultrasound Med. Biol.*, vol. 3, pp. 15-20, 1977.

[3] J. S. Bendat and A. G. Piersol, *Random Data Analysis and Measurement Procedures.* New York: Wiley, 1986, 2nd ed. ch. 1 and 11.

[4] R. N. Bracewell, *The Fourier Transform and Its Applications, 2nd ed.* New York: McGraw-Hill, 1978, Chaps. 4 and 6.

[5] T. M. Burke, M. M. Goodsitt, E. L. Madsen, and J. A. Zagzebski, "Angular distribution of scattered ultrasound from a single steel sphere in agar gelatin: a comparison between theory and experiment," *Ultrasonic Imaging*, vol. 6, pp. 342-347, 1984.

[6] J. A. Campbell and R. C. Waag, "Normalization of ultrasonic scattering measurements to obtain average differential scattering cross sections for tissues," *J. Acoust. Soc. Amer.*, vol. 74, pp. 393-399, 1983.

[7] R. E. Davidsen and S. W. Smith, "Sparse geometries for two-dimensional array transducers in volumetric imaging," *IEEE Ultrason. Symp. Proc.*, 93CH3301-9, pp. 1091-1094, 1993.

[8] J. J. Faran, "Sound scattering by solid cylinders and spheres," *J. Acoust. Soc. Amer.*, vol. 23, pp. 405-418, 1951.

[9] P. D. Freiburger, D. C. Sullivan, B. H. LeBlanc, S. W. Smith, and G. E. Trahey, "Two dimensional ultrasonic beam distortion in the breast: in vivo measurements and effects," *Ultrasonic Imaging*, vol. 14, pp. 398-414, 1992.

[10] J. W. Goodman, *Introduction to Fourier Optics.* San Francisco, CA: McGraw-Hill, 1968, ch. 3-5.

[11] M. F. Insana, R. F. Wagner, D. G. Brown, and T. J. Hall, "Describing small-scale structure in random media using pulse-echo ultrasound," *J. Acoust. Soc. Amer.*, vol. 87, pp. 179-192, 1990.

[12] M. F. Insana and T. J. Hall, "Parametric ultrasound imaging from backscatter coefficient measurements: Image formation and interpretation," *Ultrasonic Imaging*, vol. 12, pp. 245-267, 1990.

[13] M. F. Insana, J. G. Wood, and T. J. Hall, "Identifying acoustic scattering sources in normal renal parenchyma in vivo by varying arterial and ureteral pressures," *Ultrasound Med. Biol.*, vol. 18, pp. 587-599, 1992.

[14] M. F. Insana and D. G. Brown, "Acoustic scattering theory applied to soft biological tissues," in *Ultrasonic Scattering in Biological Tissues*, K.K. Shung and G.A. Thieme, Eds. Boca Raton, FL: CRC Press, 1993, pp. 75-124.

[15] A. Ishimaru, *Wave Propagation and Scattering in Random Media*, vol. 1. New York: Academic, 1978.

[16] L. E. Kinsler, A. R. Frey, A. B. Coppens, and J. V. Sanders, *Fundamentals of Acoustics*, 3rd ed. New York: Wiley, 1982.

[17] F. L. Lizzi, M. Greenebaum, E. J. Felappa, M. Elbaum and D. J. Coleman, "Theoretical framework for spectrum analysis in ultrasonic tissue characterization," *J. Acoust. Soc. Amer.*, vol. 73, pp. 1366-1373, 1983.

[18] A. Macovski, "Ultrasonic imaging using arrays," *Proc. IEEE*, vol. 67, pp. 484-495, 1979.

[19] E. L. Madsen, J. A. Zagzebski, and G. R. Frank, "Oil-in-gelatin dispersions for use as ultrasonically tissue-mimicking materials," *Ultrason. Med. Biol.*, vol. 8, pp. 277-287, 1982.

[20] E. L. Madsen, M. F. Insana, and J. A. Zagzebski, "Method of data reduction for accurate determination of acoustic backscatter coefficients," *J. Acoust. Soc. Amer.*, vol. 76, pp. 913-923, 1984.

[21] E. L. Madsen, "Method of determination of acoustic backscatter and attenuation coefficients independent of depth and instrumentation," in *Ultrasonic Scattering in Biological Tissues.* K. K. Shung and G.A. Thieme, Eds. Boca Raton, FL: CRC Press, 1993, pp. 205-249.

[22] D. Nicholas and C. R. Hill, "Evaluation of backscatter coefficients for excised human tissues: principles and techniques," *Ultrasound Med. Biol.*, vol. 8, pp. 7-15, 1982.

[23] M. O'Donnell and J. G. Miller, "Quantitative broadband ultrasonic backscatter: an approach to nondestructive evaluation in acoustically inhomogeneous materials," *J. Appl. Phys.*, vol. 52, pp. 1056-1065, 1981.

[24] H. T. O'Neil, "Theory of focusing radiators," *J. Acoust. Soc. Amer.*, vol. 21, pp. 516-526, 1949.

[25] K. J. Peters and R. C. Waag, "Compensation for receiver bandpass effects on ultrasonic backscatter power spectra using a random medium reference," *J. Acoust. Soc. Amer.*, vol. 84, pp. 392-399, 1988.

[26] K. K. Shung, "*In vitro* experimental results on ultrasonic scattering in biological tissues," in *Ultrasonic Scattering in Biological Tissues*, K. K. Shung and G. A. Thieme, Eds. Boca Raton, FL: CRC, 1993, pp. 291-312.

[27] R. A. Sigelmann and J. M. Reid, "Analysis and measurement of ultrasonic backscattering from an ensemble of scatterers excited by sine-wave bursts," *J. Acoust. Soc. Amer.*, vol. 53, pp. 1351-1355, 1973.

[28] S. W. Smith, G. E. Trahey, and O. T. von Ramm, "Two-dimensional arrays for medical ultrasound," *Ultrasonic Imaging*, vol. 14, pp. 213-233, 1992.

[29] M. Ueda and Y. Ozawa, "Spectral analysis of echoes for backscatter coefficient measurement," *J. Acoust. Soc. Amer.*, vol. 77, pp. 38-47, 1985.

[30] R. C. Waag and J. P. Astheimer, "Measurement system effects in ultrasonic scattering experiments," in *Ultrasonic Scattering in Biological Tissues*, K. K. Shung and G. A. Thieme, Eds. Boca Raton, FL: CRC, 1993, pp. 251-290.

[31] J. A. Zagzebski, L. X. Yao, E. J. Boote, and Z. F. Lu, "Quantitative

backscatter imaging," in *Ultrasonic Scattering in Biological Tissues*, K. K. Shung and G. A. Thieme, Eds. Boca Raton, FL: CRC, 1993, pp. 451-486.

[32] Given that the element pitch d equals $\lambda_0/2$ at the center frequency of the transducer, $f_0 = c/\lambda_0$, and that a high-quality saw gives an element gap of $d - w = 25\mu$m, then the approximation of (18) biases σ_b estimates less than 5% ($w/d = 1 - 2f_0(d-w)/c \geq 0.7$ in Fig. 3) when $f_0 \leq 0.3c/2(d-w) \simeq 9$ MHz. This frequency range encompasses most of diagnostic imaging. For the 5 MHz linear array used in this study, $w/d \simeq 0.83$. We estimate from the data in Fig. 3 that the measurements in Figs. 6 and 7 are biased high by only 1%.

[33] Schematics for the digital gate in Fig. 4 are available upon request. Address requests to T. J. Hall, Dept. of Radiology, KUMC, 3901 Rainbow Blvd., Kansas City, KS 66160-7234.

[34] The temperature dependence of the speed of sound in water was found using the reference by N. Bilaniuk and G. S. K. Wong, "Speed of sound in pure water as a function of temperature," *J. Acoust. Soc. Amer.*, vol. 93, pp. 1609-1612, 1993. The density of water as a function of temperature is given by G. W. C. Kaye and T. H. Laby *Tables of Physical and Chemical Constants, 15th ed.* New York: Longman, 1986, p. 29. The temperature dependence of the speed of sound of CCl_4 is given in *Handbook of Chemistry and Physics, 66th ed.* Boca Raton, FL: CRC, 1985, p. E-43, and the temperature dependence of the density of CCl_4 is given by J. A. Riddick and W. B. Bunger, *Organic Solvents: Physical Properties and Methods of Purification, 3rd ed.*, New York: Wiley, 1970, pp. 351-353. Useful linear approximations to the data for CCl_4 referenced above are ρ (g/cm^3) $= -1.9277 \times 10^{-3}\ T(^\circ C) + 1.6326$ and c (mm/μs) $= -2.70 \times 10^{-3}\ T(^\circ C) + 0.9935$.

Timothy J. Hall (M'88) was born in Flint, MI on February 16, 1956. He received the A.B. degree in physics from the University of Michigan, Flint, in 1983, and the M.S. and Ph.D. degrees in medical physics from the University of Wisconsin, Madison in 1985 and 1988, respectively.

He is currently an Assistant Professor with the Department of Radiology at the University of Kansas Medical Center. His research interests include quantitative ultrasonic imaging, and measures of observer performance and image qualtity.

Dr. Hall is a member of the Acoustical Society of America, the Society of Photo-Optical Instrumentation Engineers, the American Association of Physicists in Medicine, and the American Institute of Ultrasound in Medicine.

Larry T. Cook (S'75–M'78) received the Ph.D. degree in electrical engineering from the University of Missouri in 1978.

Since then he has been with the University of Kansas working on various aspects of electronic medical imaging, including picture archiving and communications systems, 3-D visualization, and applications of observer performance measures to radiological tasks. Currently, he is a Professor of Radiology at the University of Kansas.

Dr. Cook is a member of the AMS, SPIE, and AAAS.

Michael F. Insana (M'85) was born in Portsmouth, VA on December 18, 1954. He received the B.S. degree in physics from Oakland University, Rochester, MI in 1978 and the M.S. and Ph.D. degrees in medical physics from the University of Wisconsin, Madison, in 1982 and 1983, respectively.

From 1984 to 1987 he was a research physicist at the FDA's Center for Devices and Radiological Health, where he worked in medical imaging with emphasis on acoustic signal processing. He is currently an Associate Professor of Radiology at the University of Kansas Medical Center. His current research interests are acoustic imaging and tissue characterization, signal detection theory, observer performance measurements, and image quality assessment. He is a member of SPIE, ASA, AIUM, and AAPM professional societies.